ACS APPLIED MATERIALS & INTERFACES

Research Article

www.acsami.org

Effect of Noncovalent Basal Plane Functionalization on the Quantum Capacitance in Graphene

Mona A. Ebrish, Eric J. Olson, and Steven J. Koester*

University of Minnesota—Twin Cities, 200 Union Street SE, Minneapolis, Minnesota 55455, United States

Supporting Information

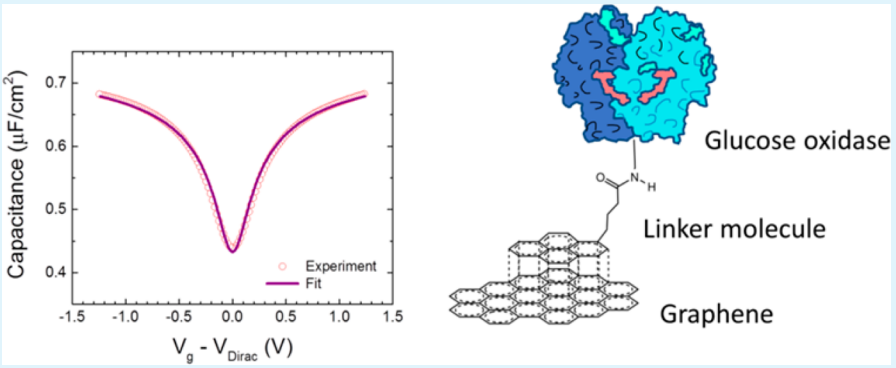

ABSTRACT: The concentration-dependent density of states in graphene allows the capacitance in metal−oxide−graphene structures to be tunable with the carrier concentration. This feature allows graphene to act as a variable capacitor (varactor) that can be utilized for wireless sensing applications. Surface functionalization can be used to make graphene sensitive to a particular species. In this manuscript, the effect on the quantum capacitance of noncovalent basal plane functionalization using 1-pyrenebutanoic acid succimidyl ester and glucose oxidase is reported. It is found that functionalized samples tested in air have (1) a Dirac point similar to vacuum conditions, (2) increased maximum capacitance compared to vacuum but similar to air, (3) and quantum capacitance "tuning" that is greater than that in vacuum and ambient atmosphere. These trends are attributed to reduced surface doping and random potential fluctuations as a result of the surface functionalization due to the displacement of H_2O on the graphene surface and intercalation of a stable H_2O layer beneath graphene that increases the overall device capacitance. The results are important for future application of graphene as a platform for wireless chemical and biological sensors.

KEYWORDS: *graphene, sensor, quantum capacitance, functionalization, glucose oxidase, varactor*

INTRODUCTION

Graphene is an attractive material for sensing applications because of its large surface-to-volume ratio and high electrical conductivity.[1] For this reason, numerous demonstrations of graphene sensors have been made in the literature.[1−7] Most of these have been based upon changes in the resistance of graphene proportional to the analyte concentration. Such applications typically require signal readout through a wired configuration, thereby greatly limiting the applicability of these sensors for long-term in vivo applications. Recently, a novel sensing mechanism[8,9] has been proposed and demonstrated based on the quantum capacitance effect in graphene.[10,11] In this technique, a molecule adsorbed onto the surface of a metal−oxide−graphene (MOG) device can change the graphene quantum capacitance by shifting the Fermi-level position relative to the Dirac energy. If the oxide thickness is small enough, the Fermi-level shift can produce a measurable change in the device capacitance. When the MOG device is integrated with an inductor, the resonant frequency of the resulting LC circuit is changed and this shift can be detected wirelessly. This technique has a compelling advantage over resistance-based sensing in that the analyte concentration is encoded as the resonant frequency of the passive oscillator circuit and thus is immune to many of the noise sources inherent in amperometric sensing. Such a sensor platform has a particular potential for in vivo applications because of its small size and passive, wireless readout capability.[8,9]

In both capacitive and resistive sensing schemes, effective surface functionalization must be developed in order to achieve sensitivity for the analyte along with selectivity over interfering species.[12−14] Such surface functionalization can be achieved by noncovalently binding a linker molecule to the graphene surface with $\pi-\pi$ interactions. For example, glucose oxidase (GOx) has previously been attached to the graphene surface in order to realize resistive glucose sensors.[2,15] In those studies, GOx was attached to the graphene surface using the linker

Received: March 21, 2014
Accepted: June 4, 2014
Published: June 4, 2014

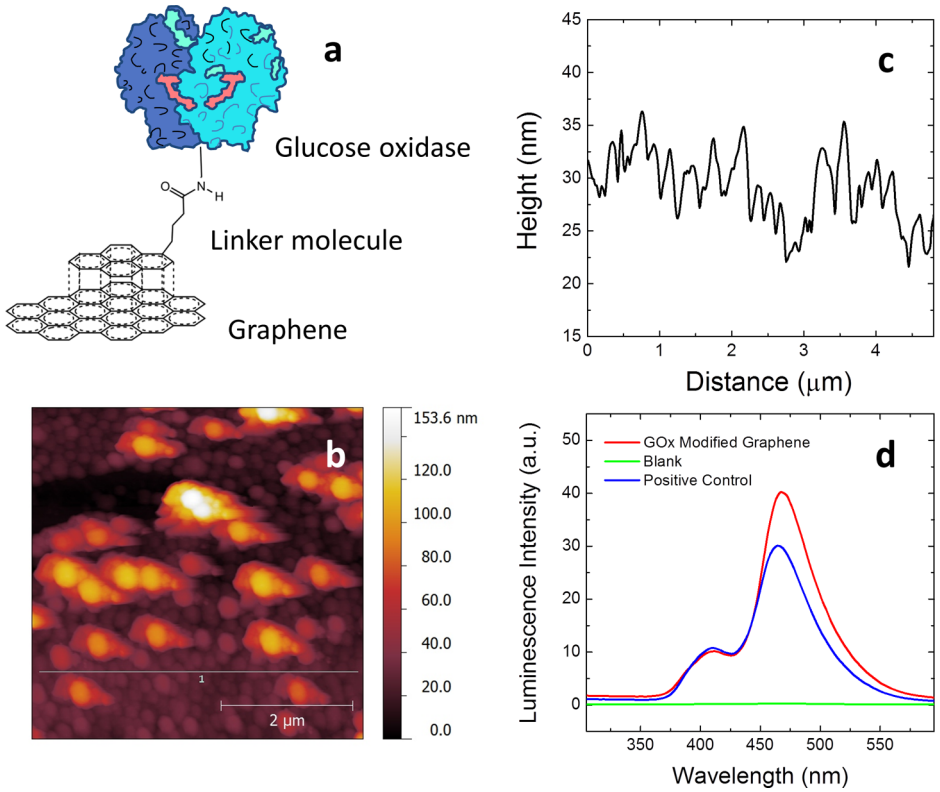

Figure 1. (a) Schematic diagram of graphene functionalization of a varactor using GOx. (b) AFM image of functionalized single-layer graphene. (c) Linescan AFM image from the sample in part b, indicating a mean height variance of 5.0 nm, consistent with the expected value of 6.2 nm for GOx. (d) Chemiluminescence spectra confirming H_2O_2 production from GOx-functionalized graphene as well as a positive control of GOx in solution.

molecule 1-pyrenebutanoic acid succimidyl ester (1-PASE; Figure 1a), and this same functionalization scheme has been utilized to create carbon nanotube glucose sensors as well.[16]

The previous results suggest the possibility that wireless glucose sensors could be achieved if 1-PASE/GOx functionalization were combined with graphene varactors. However, before such devices can be realized, developing an understanding of the effect of the functionalization process on the graphene properties is critical in order to accurately predict the capacitance and its change in response to external molecules. There are several factors that affect the capacitance in MOG varactors. First, the gate voltage at which the Fermi level is at the Dirac point needs to be known. This can be affected not only by the work function of the gate metal but also by trapped and adsorbed charges both above and below graphene. Second, disorder in graphene induced by grain boundaries and random charges can lead to the formation of electron−hole "puddles" that increase the quantum capacitance near the Dirac point. Finally, the value of the oxide capacitance itself can often have some uncertainty because of the fact that the gap between graphene and the adjacent dielectric can potentially be modified by surface functionalization and various adsorbates.[17−19]

In this work, we utilize locally back-gated MOG capacitors to study the effect of 1-PASE/GOx surface functionalization on the quantum capacitance in graphene. We find that the functionalization significantly enhances the quantum capacitance signature compared to nonfunctionalized devices measured under both ambient and vacuum conditions. These results provide important information regarding the surface interactions and adsorbate-induced disorder in functionalized and nonfunctionalized graphene devices.

RESULTS AND DISCUSSION

Functionalization Evaluation. The 1-PASE/GOx surface functionalization procedure was first evaluated on blanket graphene samples in order to independently confirm that the surface functionalization could indeed be realized. For this purpose, GOx serves as an ideal test vehicle to verify attachment of the linker molecule because the presence of GOx on the graphene surface can readily be detected using physical and chemical characterization.[2,15] In this work, functionalization was performed according to a previously reported procedure.[2,15] Briefly, single-layer graphene grown by chemical vapor deposition (CVD) on copper foil was transferred onto a Si/SiO_2 substrate using poly(methyl methacrylate) as a mechanical support.[20] The functionalization was then carried out in a three-step process: (1) physisorption of the 1-PASE linker molecule from *N*,*N*-dimethylformamide, (2) covalent attachment of GOx to the surface by aminolysis of the succinimidyl ester, and (3) deactivation of the remaining unreacted linker with ethanolamine. The molecule 1-PASE was chosen as the linker because the $\pi-\pi$ bonds have been shown to provide a stable bond to graphene and also react readily with GOx to form a covalent link to immobilize GOx on graphene.[21,22] The presence of GOx on graphene was determined by alternating-current (tapping) mode atomic force microscopy (AFM) in a desiccated atmosphere. A representative AFM image, shown in Figure 1b, shows rounded features with an average height of ∼5.0 nm, which is consistent with the known radius (6.2 nm) of GOx; however, as shown in Figure 1c, the lateral diameter of the features is significantly larger (∼100 nm) than expected.[23] This lateral distortion of the GOx molecules is likely a result of globulation of GOx during

dx.doi.org/10.1021/am5017057 | ACS Appl. Mater. Interfaces 2014, 6, 10296−10303

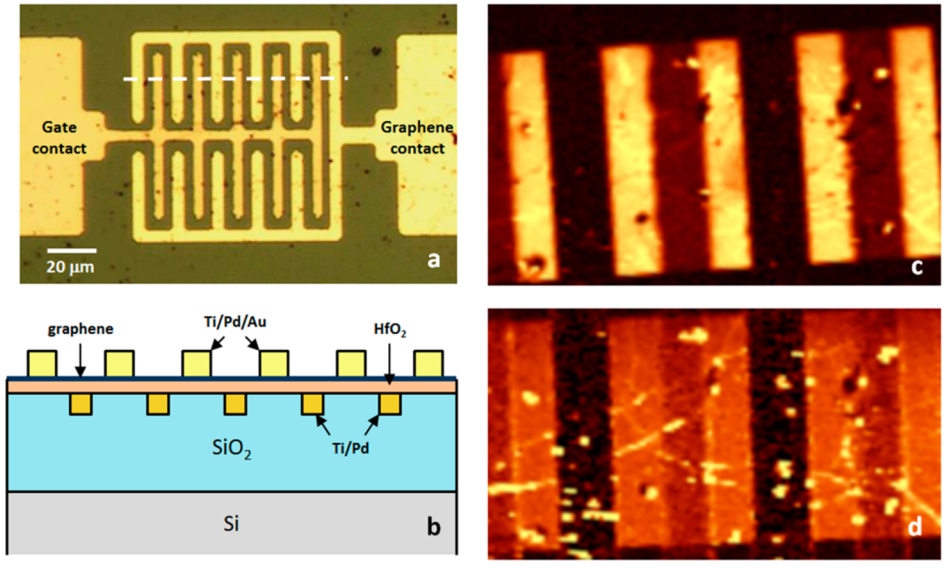

Figure 2. (a) Top-view optical micrograph of a multifinger MOG varactor. (b) Cross-sectional diagram of the device structure in (a). (c and d) Raman spectroscopic map of a portion of the graphene varactor in part a. Part c shows the G peak, while part d shows the 2D peak intensity map.

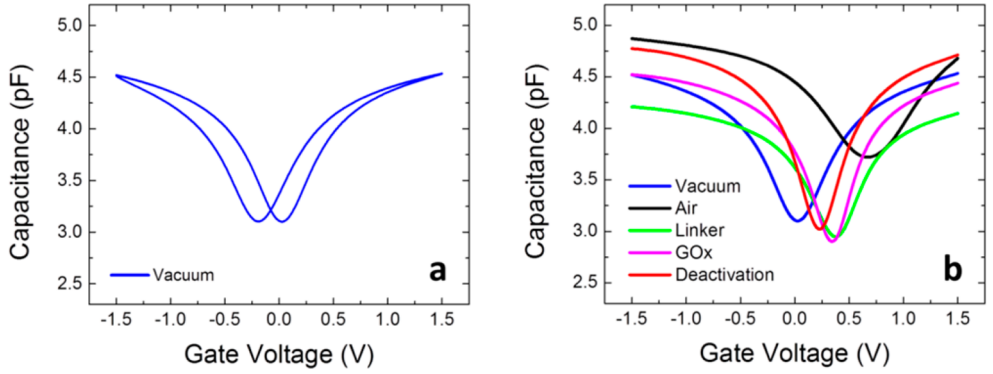

Figure 3. (a) $C-V$ curve for a typical graphene varactor measured in vacuum (before functionalization). The measurement frequency is 500 kHz, and the plots show both the up and down voltage sweeps. (b) Sequence of $C-V$ characteristics for the same device as that in part a under the following conditions: blue, vacuum before functionalization; black, ambient atmosphere before functionalization; green, ambient atmosphere after 1-PASE attachment; magenta, ambient atmosphere after GOx attachment; red, ambient atmosphere after final linker deactivation.

the immobilization and subsequent desiccation of GOx on the graphene surface. To further confirm that GOx had indeed been immobilized on graphene, the viability of GOx was confirmed by verifying the production of H_2O_2 in the presence of glucose. As shown in Figure 1d, the functionalized graphene produced a luminescence signature similar to that of the positive control solution, confirming both the presence and viability of GOx on the graphene surface.[24]

Effect of Surface Functionalization on the Capacitance. In order to test the effect of functionalization on the quantum capacitance, MOG capacitors were fabricated utilizing an inverted (graphene-on-top) geometry. The device structure has been described previously[17] and consists of a buried titanium/palladium gate electrode, a HfO_2 gate dielectric, and titanium/palladium/gold ohmic contacts to graphene. Several devices with both single-gate-finger and multifinger layouts were fabricated, and an optical micrograph and cross-sectional diagram of one such device are shown in parts a and b of Figure 2, respectively. In this geometry, the variable density of states in graphene leads to a capacitance that varies with the applied voltage between the gate and ohmic contacts. Because of the fact that the yield of the CVD graphene-transfer process is not always ideal, spatially resolved Raman spectroscopy was performed on a subset of the completed devices to provide an estimate of the active area of the devices. The Raman maps obtained for both the G and 2D peaks of a portion of a representative device are shown in parts c and d of Figure 2, respectively.

After fabrication, all devices were subjected to an extended prebake in vacuum to eliminate adsorbed H_2O. Immediately after the prebake, capacitance versus voltage ($C-V$) measurements were carried out on the devices in vacuum. A typical $C-V$ curve measured at a frequency f = 500 kHz is shown in Figure 3a. It is important to note that this plot shows some degree of hysteresis in the forward and reverse scans (see the Supporting Information for additional $C-V$ characteristics), which is characteristic of all devices and is mainly attributed to charge trapping in the HfO_2 dielectric.[25] We note that the average gate voltage at the Dirac point occurs near 0 V in vacuum, despite the fact that the work function difference between palladium (5.1 eV) and pristine graphene (4.5 eV) is ~0.6 V. We attribute this shift from the anticipated Dirac voltage to donorlike defects in amorphous HfO_2 that have been shown to slightly n-type-dope graphene[26] and therefore

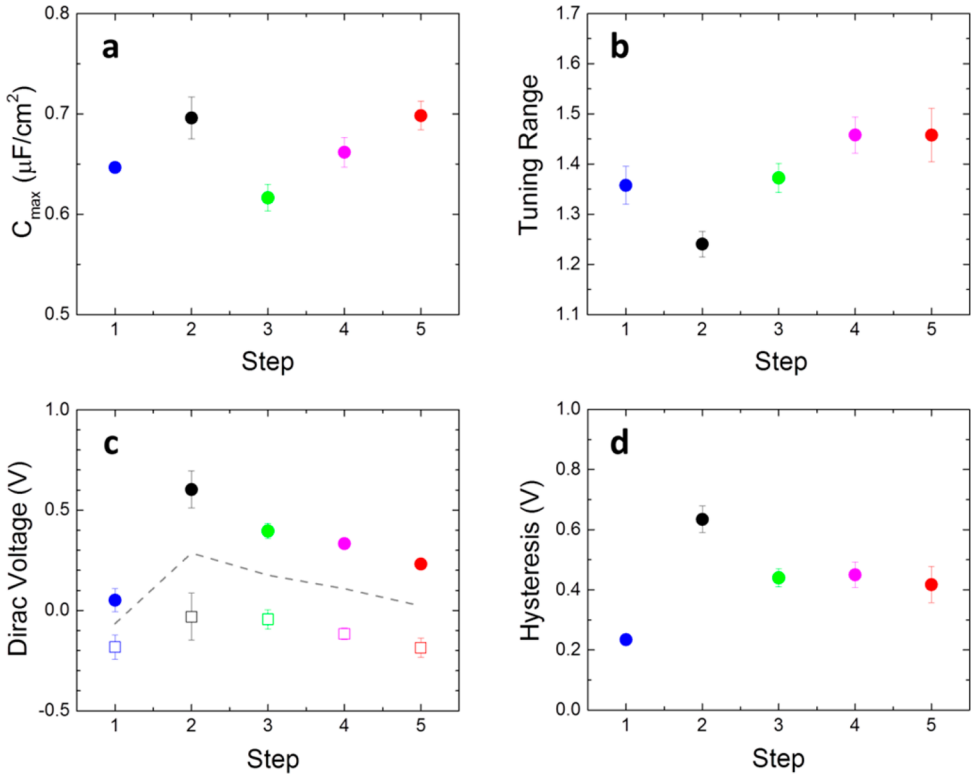

Figure 4. Plot of measured parameters compiled from seven graphene varactors as a function of the functionalization step. In this plot, the functionalization steps are numbered as follows: step 1, vacuum before functionalization; step 2, ambient atmosphere before functionalization; step 3, ambient atmosphere after 1-PASE attachment; step 4, ambient atmosphere after GOx attachment; step 5, ambient atmosphere after final linker deactivation. The measured parameters are (a) C_{max}, (b) Tuning range (C_{max}/C_{min}), (c) Dirac voltage for up (open symbols) and down (solid symbols) sweeps, as well as the average between the two (dashed line), and (d) hysteresis determined as the difference in the Dirac voltages between the up and down sweeps. The error bars indicate the standard deviation obtained over seven devices.

counteract the high work function gate metal in our samples. After measurement in vacuum, the devices were removed from the vacuum chamber, and $C-V$ measurements were repeated at each stage of surface functionalization.

The $C-V$ measurements after each stage of functionalization for a representative device are shown in Figure 3b. In these measurements, while hysteresis similar to Figure 3a was observed in all samples, only the reverse scan (V_{gs} decreasing) is shown in Figure 3b for clarity. In this figure, the $C-V$ curve measured in vacuum is shown by the blue curve, while the black curve shows the device characteristic obtained after testing immediately after removal from the vacuum chamber. Here, several features are immediately evident. First, the Dirac point shifts to a more positive voltage, indicating p-type doping relative to that of vacuum. Next, the maximum capacitance is observed to increase compared to the vacuum case. Finally, the ratio of the maximum-to-minimum capacitance, C_{max}/C_{min} (within a given gate voltage window), dramatically decreases compared to that of vacuum. The evolution of the $C-V$ characteristics after each step in the functionalization process is also shown in Figure 3b. Here, the $C-V$ characteristics were measured after attachment of the linker molecule (green), bonding of GOx to the linker molecule (magenta), and finally deactivation of the remaining unreacted linker (red). Several trends emerge throughout this sequence. First, the maximum capacitance of the fully functionalized device, while decreased slightly compared to air, remains higher than that in vacuum. Second, the Dirac point shifts back toward zero, approaching the value in vacuum. Finally, and perhaps most surprisingly, the minimum capacitance actually decreases, leading to a C_{max}/C_{min} value that exceeds the ratio in vacuum.

To confirm and quantify the trends described above, the same sequence of $C-V$ measurements was repeated for a total of seven MOG capacitors fabricated on the same wafer, including MOG capacitors of both multifinger and single-finger geometries. The average Dirac point, tuning range (C_{max}/C_{min}), maximum capacitance, and hysteresis for each step in the functionalization process are shown in Figure 4 along with error bars corresponding to the standard deviation of the measured parameters obtained over the seven measured devices. Both the forward and reverse sweeps were averaged together when extracting the tuning range, maximum capacitance, and hysteresis, while the up and down sweeps were considered independently when calculating the average Dirac point.

The plots shown in Figure 4 clearly show that the general trends described in Figure 3b are indeed systematic within experimental error. Figure 4a shows the trends in the maximum capacitance (defined as the average capacitance at $V_{gs} - V_{Dirac} = \pm 1.3$ V) after each step in the functionalization process. The devices measured in air had 0.05 μF/cm^2 higher capacitance compared to vacuum. After attachment of the 1-PASE linker, the capacitance reverted back to its vacuum value, only to increase upon complete functionalization. Figure 4b shows the capacitance tuning range (C_{max}/C_{min}) trend. After functionalization, the devices (measured in air) have $C_{max}/C_{min} = 1.46 \pm 0.05$, which is larger than that obtained in vacuum before functionalization (1.36 ± 0.04), confirming the surprising result hinted at in Figure 3b. Finally, the average value of V_{Dirac}

dx.doi.org/10.1021/am5017057 | ACS Appl. Mater. Interfaces 2014, 6, 10296−10303

(indicated by the dashed line in Figure 4c) is −0.07 V in vacuum, with a hysteresis between the up and down sweeps of 0.23 V. Upon testing in air, the average value increased to +0.29 V with a dramatic increase in hysteresis to 0.63 V. Finally, after the successive functionalization steps, the average Dirac voltage is 0.02 V, nearly the same as its original value in vacuum. In fact, the Dirac voltage of the up sweep after functionalization is nearly identical with that in vacuum. However, even after complete functionalization, a larger hysteresis (>0.4 V) remains.

Theoretical Modeling and Parameter Extraction. In order to gain further insight into the origin of the trends observed in Figure 4, theoretical fitting of the $C-V$ characteristics was performed by treating the MOG capacitor as a series circuit combination of a fixed oxide capacitance, C_{ox}, and the quantum capacitance, C_Q. In this model, the total capacitance of the circuit, C_{total}, is determined as

$$C_{total} = A[1/C_{ox} + 1/C_Q]^{-1} \quad (1)$$

where A is the total active area of graphene, which is determined using the Raman mapping shown in Figure 2. The oxide and quantum capacitance can then be calculated as

$$C_{ox} = \frac{3.9\varepsilon_0}{EOT} \quad (2)$$

and

$$C_Q = \frac{2q^2 k_B T_{eff}}{\pi(\hbar v_f)^2} \ln\left[2 + 2\cosh\left(\frac{E_F}{kT_{eff}}\right)\right] \quad (3)$$

respectively. In eq 2, EOT is the equivalent oxide thickness of the gate dielectric, and in eq 3, q is the electronic charge, k_B is Boltzmann's constant, $\hbar$ is the reduced Planck constant, $v_f = 1.1 \times 10^6$ cm/s is the Fermi velocity in graphene, and E_F is the Fermi energy relative to the Dirac point energy. In addition, we have introduced an effective temperature, T_{eff}, which is defined as

$$T_{eff} = \sqrt{T_0^2 + T^2} \quad (4)$$

where T is the measurement temperature and T_0 is a parameter that represents the magnitude of random potential fluctuations in graphene. This method of representing the potential fluctuations in graphene is equivalent to previous descriptions in the literature[17,27] (see the Supporting Information). It is important to note that the parameter EOT not only represents the actual thickness of HfO_2 but also includes the thin interfacial layer that separates graphene and HfO_2. After normalization of the capacitance to the active area, T_0 and EOT were fit by sum-of-squares optimization in *MATLAB*, and only the $C-V$ curves collected at a measurement frequency of f = 500 kHz were used for fitting purposes. An example of the fit is shown in Figure 5, where values of EOT = 4.42 nm and T_0 = 292 K were extracted for a varactor measured in an ambient atmosphere after complete functionalization.

The values for EOT and T_0 extracted from the fitting procedure are shown in Figure 6. Figure 6a shows the extracted EOT values, and in vacuum, the average value obtained is 4.70 ± 0.05 nm. Initially, upon attachment of the linker, EOT increases again but then decreases throughout the functionalization process, returning to a value (4.28 ± 0.11 nm) nearly identical with that measured in air before functionalization. In Figure 6b, the trends in the disorder parameter, T_0, are shown. In vacuum, T_0 = 479 ± 50 K, a value that corresponds to

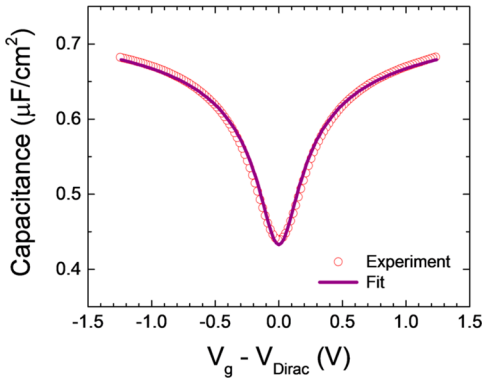

Figure 5. Plot showing a comparison of fit versus experimental $C-V$ characteristics (where the x axis has been normalized to the Dirac voltage) for one device measured after completion of the surface functionalization. The open symbols represent the experimental data, and solid line shows the theoretical result using fitting parameters of EOT = 4.42 nm and T_0 = 292 K. The R^2 value for this fit is 0.9962.

random potential fluctuations with magnitude on the order of 72 ± 15 meV, a value similar to our previous results.[17] The T_0 value increases substantially to 711 ± 70 K for unfunctionalized devices in an ambient atmosphere but decreases again upon initial attachment with 1-PASE and then remains fairly constant through the GOx attachment and deactivation steps, finally reaching T_0 = 406 ± 63 K, a value that is lower than that in vacuum. The uncertainty values for the parameters listed above represent the standard deviation of the extracted parameters obtained over the seven measured devices, where the device shown in Figure 5 had the lowest extracted value of T_0 = 292 K for any device and condition characterized in this study.

Physical Interpretation. The decrease in EOT (and the associated increase in C_{max}) in ambient atmosphere compared to vacuum is believed to be the result of a continuous film of H_2O that slowly intercalates under graphene when the device is exposed to a humid atmosphere,[28] in contrast to the situation in vacuum, where H_2O has been completely desorbed because of the long bake that was performed prior to measurement. The van der Waals interaction between graphene and HfO_2 is known to result in a gap on the order of 0.33 nm,[26] and the presence of this gap is likely one of the reasons why we have found EOT in MOG capacitors to be substantially higher than that in metal−insulator−metal capacitors.[29] In fact, because this gap region has $\varepsilon_r \sim 1$, it can increase EOT by an additional 1.3 nm compared to the situation when it was not present. However, it is expected that intercalation of H_2O into this region should substantially reduce EOT because of the very large dielectric constant (~80) of liquid H_2O. The observed decrease of EOT by 0.4 nm is consistent with this trend, although less than the expected value of >1 nm. This could be due to an increase in the gap thickness due to the physical size of the H_2O molecule as well as the fact that the dielectric constant of monolayer H_2O may not be the same as that of "bulk" liquid H_2O. Further evidence of H_2O intercalation was provided by collecting AFM images of an exfoliated graphene flake at each step of the functionalization process, which reveal a substantial decrease in the graphene−HfO_2 step height upon vacuum baking (see the Supporting Information). The AFM data from each stage of functionalization also suggest that the separation of graphene and HfO_2 decreases throughout the functionalization process. Thus, the observed decrease in EOT through functionalization, along with the relatively large

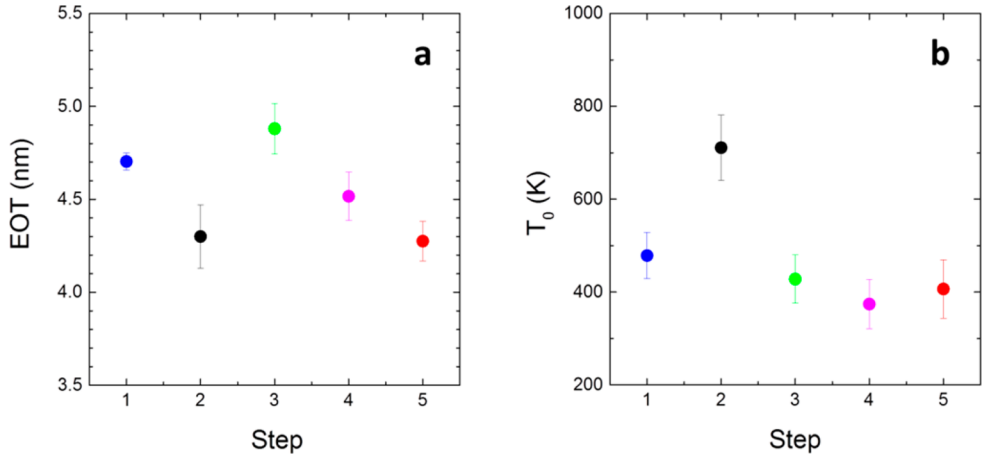

Figure 6. Plot of extracted parameters compiled from seven graphene varactors as a function of the functionalization step, where the functionalization steps are ordered the same as those in Figure 4. The extracted parameters are (a) EOT and (b) T_0. The error bars indicate the standard deviation of the extracted values obtained over seven devices.

hysteresis (compared to vacuum), suggests a combination of the effect of H_2O intercalation below graphene along with a change in the graphene−HfO_2 step height throughout functionalization.

The trends in the disorder parameter, T_0, are equally revealing regarding the effect of H_2O on the quantum capacitance properties. In vacuum, the T_0 parameter appears to be small because of the lack of H_2O vapor in the system. However, in an ambient atmosphere, H_2O is expected to not only intercalate underneath graphene but also adsorb onto the top surface of graphene. Unlike intercalated H_2O, H_2O on the top surface is expected to be randomly distributed with surface position and orientation because it maintains a steady-state condition relative to the atmosphere. Moreover, H_2O has been shown to preferentially adsorb onto oxygen-containing defect sites on graphene, as well as polymeric residues on the graphene surface left over from the transfer process.[30−33] Because adsorbed H_2O is not uniformly distributed upon the graphene surface, some areas are expected to be heavily doped by adsorbed H_2O while other areas are expected to exhibit very little doping. This hypothesis is supported by the fact that, after functionalization, T_0 is dramatically reduced. This result strongly suggests that functionalization displaces the disorder-inducing H_2O on the top surface of graphene while still allowing more ordered H_2O to remain beneath. However, it is still unclear as to why the disorder is actually lower than that measured in vacuum. One possibility is that the higher dielectric constant of the adjacent H_2O intercalated layer modifies the Fermi velocity in graphene, similar to previous studies on graphene with few-layer ice deposited on top.[34] Other works studying the effect of fluorinated polymers deposited on graphene have shown similar effects.[35] However, the origin of such effects is unclear in our samples, particularly because Raman spectroscopy on our functionalized graphene samples did not show any systematic modification as a result of the functionalization process. Therefore, further studies of the atomic-level interactions between graphene, HfO_2, and the linker molecules are needed.

Finally, the results provide additional insights into the effect of H_2O and surface functionalization on doping in graphene. First of all, the results in vacuum indicate that a "background" n-type doping exists because the expected Dirac voltage in pristine graphene is expected to be ∼0.6 V based upon the work function differences between graphene and palladium. This n-type shift is attributed to oxygen vacancies in HfO_2 that have previously been shown to shift the charge neutrality point in graphene on α-HfO_2. The trend toward more positive Dirac voltages in an ambient atmosphere is consistent with previous results that have reported a p-type doping effect associated with physisorption of H_2O. The trend toward decreasing Dirac voltage is consistent with displacement of H_2O on the graphene surface by the linker molecule. Moreover, the hydrophobicity of the local environment at the graphene surface is expected to increase as functionalization progresses, consistent with the gradually decreasing Dirac voltage. Last, the Dirac point does not completely return to the neutral point observed in vacuum, even upon full functionalization. This is consistent with intercalation of H_2O under graphene because this H_2O is expected to occupy the oxygen vacancies in HfO_2 and thus make them unavailable for doping graphene.

CONCLUSION

In conclusion, the effect of noncovalent basal plane functionalization using 1-PASE and GOx on the properties of metal−HfO_2−graphene capacitors has been studied. Three major conclusions are obtained from these experiments. The first is that the "oxide" capacitance in functionalized devices is substantially higher than that of devices measured in vacuum and comparable to devices measured in an ambient atmosphere. This is attributed to H_2O intercalation at the graphene−HfO_2 interface, which increases the dielectric constant of this interfacial region. Density functional theory and molecular dynamics simulations are currently underway to help further understand the physical nature of the HfO_2−graphene interface as well as the nature of the interaction between graphene and the linker molecules. Specifically, the cause of the observed decrease in the graphene−HfO_2 separation through the functionalization process is being investigated. Second, functionalization reduces the disorder parameter, T_0, compared to ambient atmosphere, a fact that is attributed to displacement of H_2O by the linker molecule, but the further reduction of T_0 below the value for vacuum remains unexplained. Surface functionalization does not, however, appear to otherwise alter the sp^2 nature of graphene. Finally, surface functionalization creates a Dirac voltage similar to the value obtained in vacuum, a behavior attributed to displacement

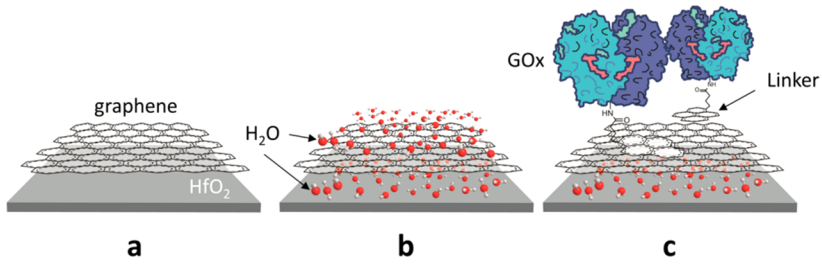

Figure 7. Pictorial diagrams of proposed mechanisms for experimentally observed behavior: (a) HfO_2−graphene interface under vacuum; (b) HfO_2−graphene interface in the presence of H_2O, showing H_2O intercalation below graphene as well as physisorbed H_2O on top of the graphene; (c) HfO_2−graphene showing that, after functionalization, H_2O can intercalate below the graphene, but functionalization prevents H_2O interaction on the graphene surface.

of H_2O on the graphene top surface (Figure 7). Further experiments are needed, however, to understand the effect of intercalated H_2O at the graphene−HfO_2 interface. For instance, AFM measurements under careful humidity control may help elucidate the change in the HfO_2−graphene spacing upon exposure to the atmosphere. The results are important for a basic understanding of surface functionalization groups for a wide range of sensor application but particularly for capacitance-based graphene sensors, and the results indicate that reproducible and stable characteristics can be obtained.

METHODS

Materials. Luminol, sodium carbonate, sodium bicarbonate, potassium ferricyanide, and glucose oxidase (GOx) type II (from *Aspergillus niger*) were purchased from Sigma-Aldrich. Glucose was purchased from Alfa Aesar. 1-Pyrenebutanoic acid succinimidyl ester (1-PASE) was purchased from AnaSpec, Inc. Single-layer graphene grown by CVD on copper foil was purchased from Graphene Laboratories. All materials were used as purchased without further purification.

Device Fabrication. The device preparation process followed a procedure similar to the one described in ref 17. Briefly, fabrication started by growing thick SiO_2 (980 nm) on a silicon wafer to minimize the parasitic capacitance with the substrate. SiO_2 was patterned and recessed using a buffered oxide etch, followed by evaporation and lift-off of a titanium/palladium (10/40 nm) gate electrode. Next, 9 nm of HfO_2 was deposited by atomic layer deposition at 300 °C and then annealed at 400 °C for 5 min. Single-layer graphene grown by CVD was then transferred onto the wafer using an aqueous transfer process. Graphene was then patterned and etched using O_2 plasma. Finally, contact electrodes to graphene consisting of titanium/palladium/gold (1/25/40 nm) were patterned and lifted off. These devices are arranged in both single-finger and multifinger geometries, with gate lengths ranging from ∼2 to 15 μm and total gate areas ranging from 155 to 1088 μm^2.

After device fabrication was completed but before functionalization, the device was baked in vacuum (∼10^{-6} Torr base pressure) at 380 K for 20 h in order to desorb moisture from the device. C−V measurements were then performed using an Agilent B1500A semiconductor parameter analyzer at frequencies f ranging from 5 to 500 kHz, using an root-mean-square oscillator voltage of 50 mV. The series equivalent circuit mode (C_s−R_s) was utilized for C−V measurements because minimal gate leakage (<1 pA) was detected in these devices over the range of gate voltages tested. Finally, the capacitance associated with the contact pads was measured and found to be negligible.

Functionalization Procedure. For functionalization, the sample was fully submerged in 5 mL of a solution of 1.93 mg/mL 1-PASE in *N*,*N*-dimethylformamide (DMF) for approximately 3 h. The sample was then rinsed by immersion in DMF, washed in deionized H_2O, and dried under a stream of nitrogen. The sample was then measured immediately after drying. To functionalize with GOx, the sample was placed in 5 mL of 10 mg/mL GOx in a pH 10 sodium carbonate buffer and refrigerated at 4 °C for approximately 14 h. The sample was then rinsed by immersion in deionized H_2O, dried under a stream of nitrogen, and measured. Finally, to deactivate the remaining unreacted linker, the sample was immersed in 0.5 M ethanolamine in a pH 10 sodium carbonate buffer solution for approximately 40 min, rinsed by immersion in deionized H_2O, dried under a stream of nitrogen, and again measured.

Determination of GOx Viability Using Luminol. In this experiment, ∼1 cm^2 pieces of graphene were transferred to an Si/SiO_2 substrate using the same method as that for the electronic devices and functionalized according to the above procedure. The functionalized graphene surface was then incubated in an approximately 2.5 mL aliquot of 5 mM glucose in 1X phosphate-buffered saline (PBS) for 1 h under static conditions. As controls, approximately 5 mg of GOx was dissolved directly in a 5 mL aliquot of a 5 mM glucose solution in PBS as a positive control and GOx was omitted from the glucose sample as a negative control. The remainder of the procedure was identical. A 1 mL aliquot of the sample fluid was then mixed with an equal volume of a 50 mM pH 10 carbonate buffer containing 2 mM luminol and 5 mM potassium ferricyanide. The emission spectrum of this solution was then immediately measured on a Jasco FP-6200 spectrofluorometer with the excitation shutter closed.

ASSOCIATED CONTENT

Supporting Information

Equivalence of approaches utilized to quantify random potential fluctuations in graphene, hysteresis and frequency dispersion in graphene varactors, and AFM studies of the effect of functionalization on the graphene−HfO_2 separation. This material is available free of charge via the Internet at http://pubs.acs.org.

AUTHOR INFORMATION

Corresponding Author

*Phone: (612) 625-1316. Fax: (612) 625-4583. E-mail: skoester@umn.edu.

Notes

The authors declare the following competing financial interest(s): S.J.K. and the University of Minnesota (UMN) have filed a patent on the portions of the technology reported here. Both UMN and S.J.K. are entitled to standard royalties should licensing revenue be generated from this invention. Currently, this technology has been licensed to Andas, Inc., and S.J.K. has a consulting relationship with Andas. No other authors declare any competing financial interests.

ACKNOWLEDGMENTS

The authors acknowledge Yoska Anugrah for assistance with the graphene exfoliation utilized in the AFM experiments. This work is supported by the Minnesota Partnership for

Biotechnology and Medical Genomics Decade of Discovery in Diabetes Program. Parts of this work were carried out in the Minnesota Nanofabrication Center, which receives partial support from the National Science Foundation (NSF) through the NNIN program, and the Characterization Facility, which is a member of the NSF-funded Materials Research Facilities Network via the MRSEC program.

REFERENCES

(1) Schedin, F.; Geim, A. K.; Morozov, S. V.; Hill, E. W.; Blake, P.; Katsnelson, M. I.; Novoselov, K. S. Detection of Individual Gas Molecules Adsorbed on Graphene. *Nat. Mater.* **2007**, *6*, 652−655.

(2) Kwak, Y. H.; Choi, D. S.; Kim, Y. N.; Kim, H.; Yoon, D. H.; Ahn, S.-S.; Yang, J.-W.; Yang, W. S.; Seo, S. Flexible Glucose Sensor Using CVD-Grown Graphene-Based Field Effect Transistor. *Biosens. Bioelectron.* **2012**, *37*, 82−87.

(3) Pearce, R.; Iakimov, T.; Andersson, M.; Hultman, L.; Spetz, A. L.; Yakimova, R. Epitaxially Grown Graphene Based Gas Sensors for Ultra Sensitive NO_2 Detection. *Sens. Actuators, B* **2011**, *155*, 451−455.

(4) Rajapitamahuni, A.; Hoffman, J.; Ahn, C. H.; Hong, X. Examining Graphene Field Effect Sensors for Ferroelectric Thin Film Studies. *Nano Lett.* **2013**, *13*, 4374−4379.

(5) Kuila, T.; Bose, S.; Khanra, P.; Mishra, A. K.; Kim, N. H.; Lee, J. H. Recent Advances in Graphene-Based Biosensors. *Biosens. Bioelectron.* **2011**, *26*, 4637−4648.

(6) Yang, G.; Lee, C.; Kim, J.; Ren, F.; Pearton, S. J. Flexible Graphene-Based Chemical Sensors on Paper Substrates. *Phys. Chem. Chem. Phys.* **2013**, *15*, 1798−1801.

(7) Hill, E. Graphene Sensors. *IEEE Sens. J.* **2011**, *11*, 3161−3170.

(8) Deen, D. A.; Olson, E. J.; Ebrish, M. A.; Koester, S. J. Graphene-Based Quantum Capacitance Wireless Vapor Sensors. *IEEE Sens. J.* **2014**, *14*, 1459−1466.

(9) Koester, S. J. High Quality Factor Graphene Varactors for Wireless Sensing Applications. *Appl. Phys. Lett.* **2011**, *99*, 163105.

(10) Xia, J.; Chen, F.; Li, J.; Tao, N. Measurement of the Quantum Capacitance of Graphene. *Nat. Nanotechnol.* **2009**, *4*, 505−509.

(11) Xu, H.; Zhang, Z.; Wang, Z.; Wang, S.; Liang, X.; Peng, L.-M. Quantum Capacitance Limited Vertical Scaling of Graphene Field-Effect Transistor. *ACS Nano* **2011**, *5*, 2340−2347.

(12) Wang, X.; Li, X.; Zhang, L.; Yoon, Y.; Weber, P. K.; Wang, H.; Guo, J.; Dai, H. N-Doping of Graphene through Electrothermal Reactions with Ammonia. *Science* **2009**, *324*, 768−771.

(13) Stine, R.; Mulvaney, S. P.; Robinson, J. T.; Tamanaha, C. R.; Sheehan, P. E. Fabrication, Optimization, and Use of Graphene Field Effect Sensors. *Anal. Chem.* **2013**, *85*, 509−521.

(14) Georgakilas, V.; Otyepka, M.; Bourlinos, A. B.; Chandra, V.; Kim, N.; Kemp, K. C.; Hobza, P.; Zboril, R.; Kim, K. S. Functionalization of Graphene: Covalent and Non-Covalent Approaches, Derivatives and Applications. *Chem. Rev.* **2012**, *112*, 6156−6214.

(15) Huang, Y.; Dong, X.; Shi, Y.; Li, C. M.; Li, L.-J.; Chen, P. Nanoelectronic Biosensors Based on CVD Grown Graphene. *Nanoscale* **2010**, *2*, 1485−1488.

(16) Cella, L. N.; Chen, W.; Myung, N. V.; Mulchandani, A. Single-Walled Carbon Nanotube-Based Chemiresistive Affinity Biosensors for Small Molecules: Ultrasensitive Glucose Detection. *J. Am. Chem. Soc.* **2010**, *132*, 5024−5026.

(17) Ebrish, M. A.; Shao, H.; Koester, S. J. Operation of Multi-Finger Graphene Quantum Capacitance Varactors Using Planarized Local Bottom Gate Electrodes. *Appl. Phys. Lett.* **2012**, *100*, 143102.

(18) Galitski, V.; Adam, S.; Das Sarma, S. Statistics of Random Voltage Fluctuations and the Low-Density Residual Conductivity of Graphene. *Phys. Rev. B* **2007**, *76*, 245405.

(19) Du, X.; Skachko, I.; Barker, A.; Andrei, E. Y. Approaching Ballistic Transport in Suspended Graphene. *Nat. Nanotechnol.* **2008**, *3*, 491−495.

(20) Suk, J. W.; Kitt, A.; Magnuson, C. W.; Hao, Y.; Ahmed, S.; An, J.; Swan, A. K.; Goldberg, B. B.; Ruoff, R. S. Transfer of CVD-Grown Monolayer Graphene onto Arbitrary Substrates. *ACS Nano* **2011**, *5*, 6916−6924.

(21) Rodríguez-López, J.; Ritzert, N. L.; Mann, J. A.; Tan, C.; Dichtel, W. R.; Abruña, H. D. Quantification of the Surface Diffusion of Tripodal Binding Motifs on Graphene Using Scanning Electrochemical Microscopy. *J. Am. Chem. Soc.* **2012**, *134*, 6224−6236.

(22) Mann, J. A.; Rodríguez-López, J.; Abruña, H. D.; Dichtel, W. R. Multivalent Binding Motifs for the Noncovalent Functionalization of Graphene. *J. Am. Chem. Soc.* **2011**, *133*, 17614−17617.

(23) Libertino, S.; Aiello, V.; Scandurra, A.; Renis, M.; Sinatra, F. Immobilization of the Enzyme Glucose Oxidase on Both Bulk and Porous SiO_2 Surfaces. *Sensors* **2008**, *8*, 5637−5648.

(24) Bostick, D. T.; Hercules, D. M. Quantitative Determination of Blood Glucose Using Enzyme Induced Chemiluminescence of Luminol. *Anal. Chem.* **1975**, *47*, 447−452.

(25) Xiong, K.; Robertson, J.; Gibson, M. C.; Clark, S. J. Defect Energy Levels in HfO_2 High-Dielectric-Constant Gate Oxide. *Appl. Phys. Lett.* **2005**, *87*, 183505.

(26) Scopel, W. L.; Fazzio, A.; Miwa, R. H.; Schmidt, T. M. Graphene on Amorphous HfO_2 Surface: An ab initio Investigation. *Phys. Rev. B* **2013**, *87*, 165307.

(27) Xu, H.; Zhang, Z.; Peng, L.-M. Measurements and Microscopic Model of Quantum Capacitance in Graphene. *Appl. Phys. Lett.* **2011**, *98*, 133122.

(28) Lee, M. J.; Choi, J. S.; Kim, J.-S.; Byun, I.-S.; Lee, D. H.; Ryu, S.; Lee, C.; Park, B. H. Characteristics and Effects of Diffused Water between Graphene and a SiO_2 Substrate. *Nano Res.* **2012**, *5*, 710−717.

(29) Ebrish, M. A.; Deen, D. A; Koester, S. J. Border Trap Characterization in Metal-Oxide-Graphene Capacitors with HfO_2 Dielectrics. *71st Device Research Conference (DRC)*, Notre Dame, IN, June 24−26, 2013.

(30) Kumar, B.; Min, K.; Bashirzadeh, M.; Barati Farimani, A.; Bae, M.-H.; Estrada, D.; Kim, Y. D.; Yasaei, P.; Park, Y. D.; Pop, E.; Aluru, N. R.; Salehi-Khojin, A. The Role of External Defects in Chemical Sensing of Graphene Field. *Nano Lett.* **2013**, *13*, 1962−1968.

(31) Dan, Y.; Lu, Y.; Kybert, N. J.; Luo, Z.; Johnson, A. T. C. Intrinsic Response of Graphene Vapor Sensors. *Nano Lett.* **2009**, *9*, 1472−1475.

(32) Pirkle, A.; Chan, J.; Venugopal, A.; Hinojos, D.; Magnuson, C. W.; McDonnell, S.; Colombo, L.; Vogel, E. M.; Ruoff, R. S.; Wallace, R. M. The Effect of Chemical Residues on the Physical and Electrical Properties of Chemical Vapor Deposited Graphene Transferred to SiO_2. *Appl. Phys. Lett.* **2011**, *99*, 122108.

(33) Rezania, B.; Dorn, M.; Severin, N.; Rabe, J. P. Influence of Graphene Exfoliation on the Properties of Water-Containing Adlayers Visualized by Graphenes and Scanning Force Microscopy. *J. Colloid Interface Sci.* **2013**, *407*, 500−504.

(34) Jang, C.; Adam, S.; Chen, J.-H.; Williams, E. D.; Das Sarama, S.; Fuhrer, M. S. Tuning the Effective Fine Structure Constant in Graphene: Opposing Effects of Dielectric Screening on Short- and Long-Range Potential Scattering. *Phys. Rev. Lett.* **2008**, *101*, 146805.

(35) Ha, T.-J.; Lee, J.; Akinwander, D.; Dodabalapur, A. The Restorative Effect of Fluoropolymer Coating on Electrical Characteristics of Graphene Field-Effect Transistors. *IEEE Electron Device Lett.* **2013**, *34*, 559−561.